Science and Technology of Advanced Materials

ISSN: 1468-6996 (Print) 1878-5514 (Online) Journal homepage: http://www.tandfonline.com/loi/tsta20

Thermal stability and phase transformations of martensitic Ti–Nb alloys

Matthias Bönisch, Mariana Calin, Thomas Waitz, Ajit Panigrahi, Michael Zehetbauer, Annett Gebert, Werner Skrotzki & Jürgen Eckert

To cite this article: Matthias Bönisch, Mariana Calin, Thomas Waitz, Ajit Panigrahi, Michael Zehetbauer, Annett Gebert, Werner Skrotzki & Jürgen Eckert (2013) Thermal stability and phase transformations of martensitic Ti–Nb alloys, Science and Technology of Advanced Materials, 14:5, 055004, DOI: 10.1088/1468-6996/14/5/055004

To link to this article: http://dx.doi.org/10.1088/1468-6996/14/5/055004

OPEN ACCESS
IOP PUBLISHING
SCIENCE AND TECHNOLOGY OF ADVANCED MATERIALS
Sci. Technol. Adv. Mater. **14** (2013) 055004 (9pp)
doi:10.1088/1468-6996/14/5/055004

Thermal stability and phase transformations of martensitic Ti–Nb alloys

Matthias Bönisch[1], Mariana Calin[1], Thomas Waitz[2], Ajit Panigrahi[2], Michael Zehetbauer[2], Annett Gebert[1], Werner Skrotzki[3] and Jürgen Eckert[1,4]

[1] IFW-Dresden, PO Box 270116, D-01171 Dresden, Germany
[2] University of Vienna, Faculty of Physics, A-1090 Vienna, Austria
[3] TU Dresden, Institut für Strukturphysik, D-01062 Dresden, Germany
[4] TU Dresden, Institut für Werkstoffwissenschaft, D-01062 Dresden, Germany

E-mail: m.boenisch@ifw-dresden.de

Received 20 May 2013
Accepted for publication 29 August 2013
Published 27 September 2013
Online at stacks.iop.org/STAM/14/055004

Abstract
Aiming at understanding the governing microstructural phenomena during heat treatments of Ni-free Ti-based shape memory materials for biomedical applications, a series of Ti–Nb alloys with Nb concentrations up to 29 wt% was produced by cold-crucible casting, followed by homogenization treatment and water quenching. Despite the large amount of literature available concerning the thermal stability and ageing behavior of Ti–Nb alloys, only few studies were performed dealing with the isochronal transformation behavior of initially martensitic Ti–Nb alloys. In this work, the formation of martensites (α' and α'') and their stability under different thermal processing conditions were investigated by a combination of x-ray diffraction, differential scanning calorimetry, dilatometry and electron microscopy. The effect of Nb additions on the structural competition in correlation with stable and metastable phase diagrams was also studied. Alloys with 24 wt% Nb or less undergo a $\alpha'/\alpha'' \rightarrow \alpha + \beta \rightarrow \beta$ transformation sequence on heating from room temperature to 1155 K. In alloys containing >24 wt% Nb α'' martensitically reverts back to β_0, which is highly unstable against chemical demixing by formation of isothermal ω_{iso}. During slow cooling from the single phase β domain α precipitates and only very limited amounts of α'' martensite form.

Keywords: titanium, niobium, martensite, thermal stability, differential scanning calorimetry, dilatometry, biomedical applications

1. Introduction

Titanium-based materials offer a wide range of adaptable structures for use in a variety of medical applications. Metastable Ti-based alloys possess a number of significant advantages that arise from their capacity to attain numerous combinations of mechanical properties by proper control of phase transformations during thermomechanical processing [1–3]. Interest in β-type Ti-based alloys as biomaterials was derived from the excellent combination of a high mechanical resistance with low elastic modulus (E) close to that of human bone ($E = 2$–30 GPa), leading to the improvement of bone remodeling and osseointegration processes [4]. These elastic properties can be reached using both lowering of the intrinsic modulus by specific chemical alloying [5] and superelastic effects associated with a

martensitic phase transformation from the high temperature bcc β phase to the orthorhombic α'' martensite [3].

Much research effort is currently dedicated to the development of new Ni-free Ti-based shape memory alloys (SMAs) with improved biological and biomechanical properties. The major problem facing the development of new biomedical SMAs is inducing shape memory (SM) behavior and superelasticity (SE) without using any harmful alloying additions. The ideal alloying additions for a biocompatible Ti-based SMA should not only improve SM and SE properties toward those of commercial Ti–Ni alloys but must also be biocompatible (i.e. without Ni, V, Al, etc) to avoid any adverse reaction of the human body.

The SM effect and SE have been reported in Ti–Mo [6], Ti–V [7] and Ti–Nb [8] alloys. However, the Ti–Mo based alloys are susceptible to ω phase embrittlement. The Ti–V alloys are not suitable for biomaterial because of the cytotoxity of V [9].

Ti–Nb based alloys are versatile candidate materials for biomedical applications for a number of reasons, including:

(i) Excellent corrosion resistance, resulting in reduced ion release in the human body environment, and increased biocompatibility, implicitly.
(ii) Good ductility to allow producing/processing of precise and versatile geometries of medical devices and adequate toughness to survive typical damage during use.
(iii) Lower Young's (elastic) modulus for certain compositions. The composition dependence of Young's modulus (E) for Ti–Nb alloys quenched from the β phase region exhibits two minima at 15 and 40 wt% Nb [10]. According to Hanada *et al* [10] the decrease of E to ~60 GPa may be the result of the suppression of the athermal $\beta \rightarrow \omega_{\text{ath}}$ transformation by quenching from the β phase region at high temperatures. Further lowering of E by alloying with additional elements [11] will render such alloys more suitable for orthopedic implants. The low stiffness/E allows proper mechanical stimulation of bone tissue surrounding the implant to reduce bone resorption, thereby ensuring the long-term fixation of the implant [4].
(iv) The thermoelastic martensitic transformation from the high temperature bcc β-phase to the orthorhombic α''-phase gives rise to superelastic and SM behavior [12]. For the vast majority of SE and SM applications in biomedicine Ti–Ni-based alloys are utilized [13]. However, the long-term contact of Ni with the human body is associated with adverse effects, such as allergic reactions.

Ti–Nb-based alloys have received the most rigorous attention over the last years. Initial focus was centered on decreasing the stiffness by appropriate ternary additions but more recently, the focus was shifted on improving the SM and SE behaviors by controlling their microstructural stability under thermomechanical processing. Many publications can be found aiming at the development of Ni-free Ti–Nb-based alloys that show SM/SE behavior and/or low E [8, 14–18]. In both cases the relevant properties can be significantly altered by thermo (mechanical) treatments. For instance, additional decrease of the elastic modulus can be achieved from the ability of the Ti–Nb-based alloys to undergo different solid-state phase transformations during deformation and/or quenching. Depending on the degree of stabilization of the parent high-temperature bcc β ($Im\bar{3}m$) solid solution the following phase transformations may occur upon rapid cooling: $\beta \rightarrow \alpha'$, $\beta \rightarrow \alpha''$ and $\beta \rightarrow \omega_{\text{ath}}$. α' (hexagonal, $P6_3/mmc$) and α'' (base-centered orthorhombic, $Cmcm$) form martensitically from the parent β phase. The non-compact hexagonal phase called ω ($P6/mmm$) can form in three ways: (a) by a displacive shuffle dominated mechanism during rapid cooling/quenching (ω_{ath}), (b) during isothermal holding at temperatures below 758 K in the case of Ti–Nb (ω_{iso}) and (c) by application of pressure [19, 20].

Decomposition of the martensites α' and α'' or of metastable β phase by ageing usually leads to lower-energy phase mixtures [21]. However, at low temperatures this decomposition becomes sluggish.

The thermal stability and phase evolution during ageing of martensitic Ti–Nb alloys has been investigated by a number of authors by various techniques, such as calorimetry, dilatometry, x-ray diffraction, electron microscopy or hardness measurements [8, 10, 22–26].

Moffat and Larbalestier [22] described the ageing process of Ti–Nb alloys as a competition between precipitating α and isothermal ω_{iso}. The resulting microstructures are highly sensitive to the thermal history. Ageing of quenched Ti–32.7Nb and Ti–39.3Nb at 673 K resulted in extensive ω_{iso} formation, whereas ageing at 673 K without prior quenching resulted in the formation of α phase. Mantani and Tajima [23] used differential scanning calorimetry (DSC), x-ray diffraction (XRD) and hardness measurements to study the ageing behavior of four different quenched Ti–Nb alloys. To extend the accessible superelastic strain various authors experimented with ageing treatments to create ω_{iso} or α precipitates in order to increase the yield strength for plastic slip of the bcc-β matrix [8, 24]. However it is well established that ω precipitates, both athermal and isothermal ones, strongly increase the Young's modulus [10] and at the same time reduce the ductility [25]. Precipitation of α or ω_{iso} enriches β in solute atoms resulting in suppression of martensitic transformation temperatures that are critical to remain constant for a cyclic stable SM effect [27]. Prolonged ageing of $\beta + \omega_{\text{iso}}$ phase mixtures can cause heterogeneous nucleation of α from ω_{iso} precipitates leading to a fine dispersion of nanometer sized α domains [28].

Despite the large amount of literature available, the Ti–Nb alloy system still remains challenging and many questions are open. Because the establishment of true equilibrium at temperatures below 800 K is virtually impossible only calculated phase boundaries are available for low temperatures [11]. The occurrence of numerous metastable phases and sluggish atomic diffusion [29] results in complex interplays and transformation behaviors. Our study aims to contribute to the understanding of the governing microstructural phenomena during various heat treatments of martensitic Ti–Nb alloys.

Table 1. Nb and O contents of the as-cast alloys. The fraction of Ti is the balance to 100 wt%.

	Analysis results	
Nominal composition (wt%)	Nb (wt%)	O (wt%)
Ti–14Nb	13.7	0.097
Ti–16.5Nb	16.1	0.103
Ti–19Nb	18.6	0.082
Ti–21.5Nb	21.1	0.082
Ti–24Nb	23.5	0.139
Ti–26.5Nb	26.2	0.129
Ti–29Nb	28.5	0.099

In this present paper, the thermal stability and phase transformations in eight martensitic (as-quenched) Ti–Nb alloys, with Nb 29 wt%, were investigated in detail using a combination of scanning calorimetry, dilatometry, XRD and transmission electron microscopy. The effect of Nb additions on the phase constitution and structural competition in correlation with stable and metastable binary phase diagrams has also been studied. Such knowledge is essential for the development of new heat treatment protocols and establishing reasonable production processes for biomedical Ti–Nb devices.

2. Experimental

Seven binary Ti–Nb master alloys of nominal Nb contents (14, 16.5, 19, 21.5, 24, 26.5, 29, 31.5) wt% were prepared by arc melting high purity elements (99.99%) under a Ti-gettered argon atmosphere. To completely dissolve the Nb pieces the ingots were remelted 5–10 times. From these master alloys, cast bulk cylinders with 10 mm diameter and up to 180 mm length were obtained using a cold-crucible casting device. The Nb and O contents in the as-cast alloys were measured by inductively coupled plasma-optical emission spectroscopy and hot gas extraction, respectively. The results are presented in table 1. In order to ensure an optimal structural homogeneity, the as-cast cylinders/rods were subjected to a homogenization heat treatment and subsequent water quenching (HOM + WQ treatment). The rods were encapsulated in quartz tubes in a 150 mbar Ar atmosphere and solution treated for 86 400 s at 1273 K in the single β-phase field. This was followed by quickly immersing the rods into water by breaking the quartz tubes in water. XRD of the as-quenched material was performed in transmission geometry in a STOE Stadi P diffractometer with Mo-Kα_1 radiation using a step size of 0.2° (2θ) and a holding time of 300 s per step. SEM specimens were prepared by glow discharge sputtering in Ar-plasma using a GD OES Spectrometer (GDA 650, Spectruma Analytic GmbH) and analyzed with a field emission gun scanning electron microscope (FEG SEM LEO 1530) operated at 15 kV. The thermal stability of as-quenched material was studied with a Netzsch DSC404 differential scanning calorimeter (10 K min^{-1} heating and cooling rate), as well as with a Netzsch DIL204c dilatometer (5 K min^{-1} heating and cooling rate). Specimens for additional heat treatments were checked

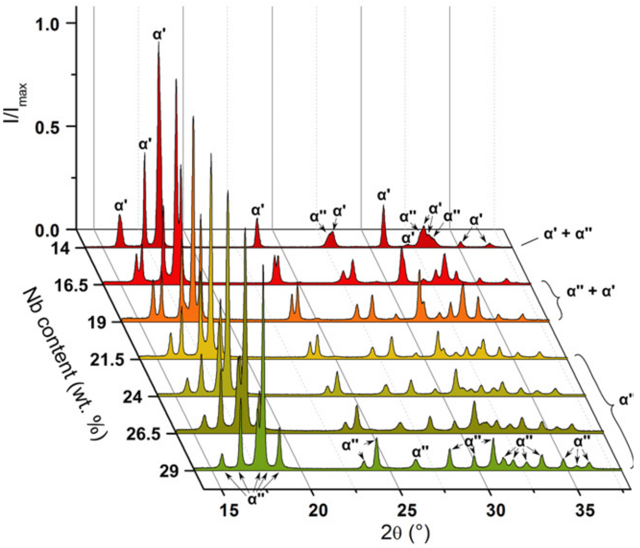

Figure 1. XRD-patterns of homogenized and water-quenched Ti–(14–29)Nb alloys.

for structural homogeneity by XRD prior to heat treatment. Afterwards each specimen was enclosed in a quartz tube under 150 mbar Ar and placed into a preheated furnace. On reaching the final temperature the specimen was quenched into water by breaking the quartz tube and re-examined by XRD. Analyses by XRD prior to and after heat treatment were carried out in reflection mode in an X'Pert PRO MPD device equipped with a PW3015 diffractometer using Co-Kα radiation with a step size of 0.02° (2θ) and a holding time of 500 s per step. TEM specimens were prepared by focused ion beam in a FEI HELIOS NanoLab 600i and studied with a Philips CM 200 microscope operated at 200 kV. Qualitative and semi-quantitative phase analysis was performed with the HighScore X'Pert software. Throughout the paper phase constitutions are denoted in the order of decreasing phase volume fractions.

3. Results and discussion

3.1. Initial phase constitution

The microstructure and phase analyses of the eight binary alloys were carried out by XRD and electron microscopy. Figure 1 shows the XRD—patterns of HOM + WQ Ti–Nb alloys. All alloys consisted primarily of martensitic phases and no additional peaks of equilibrium phases α and β were detected. That suggests the complete transformation of β phase during rapid cooling/water quenching into metastable martensitic phases, i.e. $\beta \rightarrow \alpha'/\alpha''$. The phase constitutions and structure of martensites in rapidly cooled β-stabilized Ti-based alloys is considerably influenced by the amount of solute atoms [3, 30]. Both martensite phases, α' and α'', were formed during WQ. However, higher Nb content results in the formation of α'', in preference to α'. The transition from hexagonal α' to orthorhombic α'' martensite was found to lie between 14 and 16.5 wt% Nb. Our values are in good agreement with the interval of 9.3–17.7 wt% Nb for the α'/α''

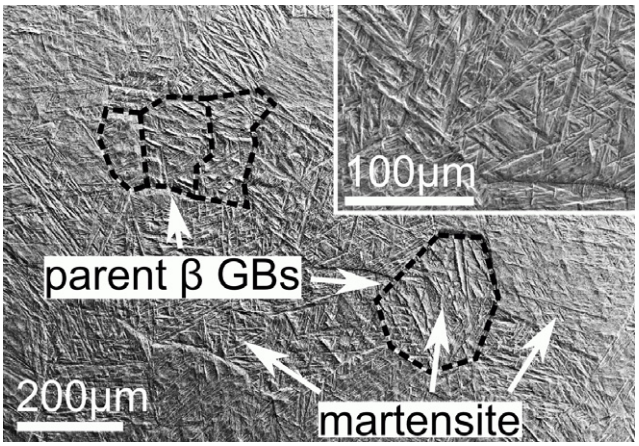

Figure 2. Secondary electron SEM micrograph of the as-quenched Ti–19Nb alloy illustrating the needle-like morphology of martensitic microstructure. GBs: grain boundaries.

transition reported in literature [31, 32]. The martensites morphology was studied by SEM, as illustrated by figure 2, which presents a typical representative SEM micrograph showing the needle-like (acicular) morphology of martensites formed during WQ. It has to be pointed out that XRD and SEM analyses of as-quenched specimens did not show the presence of ω, though the occurrence of marginal ω volume fractions or nanometer sized ω domains cannot be ruled out in regards of the experimental detection limits.

3.2. Thermal stability of the martensitic phases

The α' and α'' martensitic phases have been observed in several commercially important α and $\alpha+\beta$ alloys [1]. The SM and SE effects in several Ni-free β-stabilized Ti-alloys are based on the formation and reversion of the orthorhombic α'' phase [3, 14] and therefore profound knowledge about the conditions of α'' formation and its stability are crucial. The thermal stability of martensitic Ti–Nb alloys was investigated by DSC and dilatometry methods. Figure 3 presents the results of isochronal DSC measurements at 10 Kmin^{-1} heating and cooling rate. One DSC cycle comprised heating from room temperature (RT) to 1420 K and subsequent cooling down to RT. For each alloy two cycles were run in order to identify irreversible reactions. The temperature of 758 K below which metastable ω can exist is marked by a vertical bar. In general the thermal stability of the initially martensitic state tends to decrease and the transformation behavior becomes more complex with addition of Nb on heating, as illustrated by figure 3(a). In Ti–14Nb only one endothermic reaction (labeled I) occurring over a broad temperature range of about 200 K is detected in the first heating. This peak coincides with the β-transus, as seen by comparison with the phase diagram [11]. Addition of Nb causes the peak to shift gradually down and a small exothermic reaction to be triggered below it. This reaction (labeled II) has been identified with the decomposition of the metastable martensitic state into α and β. A drastic change of transformation behavior can be observed in alloys containing more than 26.5 wt% Nb. In these compositions an additional sharp endothermic reaction (labeled VI) corresponding to the reverse martensitic transformation $\alpha'' \rightarrow \beta_0$ is seen. The respective values for the austenite start temperature A_s of 643±3 and 577 ± 3 K for Ti–26.5Nb and Ti–29Nb obtained in this study are in good agreement with results from Jepson *et al* [33], who used higher heating rates and thus obtained values about 15 K higher. Reversion of α'' to β_0 is immediately followed by an exothermic reaction (labeled V) that results from the formation of ω_{iso}. In Ti–(26.5–31.5)Nb endothermic peaks (labeled IV) are seen at around 758 K, i.e. the maximum temperature of stability of ω in Ti–Nb [11]. Thus peaks IV were interpreted to originate from the $\omega_{iso} \rightarrow \beta$ transformation. The freshly formed β is unstable against precipitation of α as seen from peaks III. The transformation behavior during cooling shows less complexity, as can be seen from figure 3(b). In Ti–(14–29)Nb an exothermic reaction (labeled VII) is detected, the peak temperature of which is shifted down by addition of Nb. It was identified as the diffusional $\beta \rightarrow \alpha$ reaction. An additional exothermic reaction tentatively ascribed to $\beta \rightarrow \omega_{iso}$ (labeled VIII) appears in Ti–29Nb. The following part of the paper presents and discusses the experimental evidence that facilitated interpretation of DSC-scans.

3.3. Correlation of DSC and dilatometry with stable and metastable phase diagrams

In order to explain and understand the features seen in DSC, three alloys, Ti–14Nb, Ti–21.5Nb and Ti–19Nb, were chosen for more detailed investigations by complementary dilatometry and post-heat treatment XRD measurements. The phase diagrams from Zhang *et al* [11], the most recent ones to our knowledge, were employed for these purposes. Specimens of the chosen alloy were heat treated to selected temperatures, corresponding to prominent features seen in DSC-scans, see table 2. The phase constitution at the final temperature was 'frozen in' by immediately quenching the specimen into water and afterwards investigated by XRD. Special care was taken that the initial phase constitution of all samples for each alloy was identical by verifying it beforehand by XRD.

3.3.1. Ti–14Nb. Figure 4 shows the first cycles of DSC- and dilatometry-scans of Ti–14Nb together with the α/β and ω/β phase diagrams of Ti–Nb. The broad endotherm between 920 and 1120 K lies on the boundary of the $\alpha+\beta$ miscibility gap and the single β-phase region. It can be speculated whether the initial martensitic state is stable up to the endothermic peak. During the second heating, slightly less heat was released between 770 and 970 K, suggesting decomposition of the martensitic state into $\alpha+\beta$ during the first heating. Taking into account that during heating through the miscibility gap α is continuously converted into β thereby increasing the fraction of β, the broad temperature interval of about 200 K from the beginning to the end of the reaction can be understood. To identify the exothermic reaction during cooling from 1120 to 820 K the phase constitution was checked by XRD after one DSC cycle, as illustrated by figure 5(a). A mixture of α and β phases was found, the

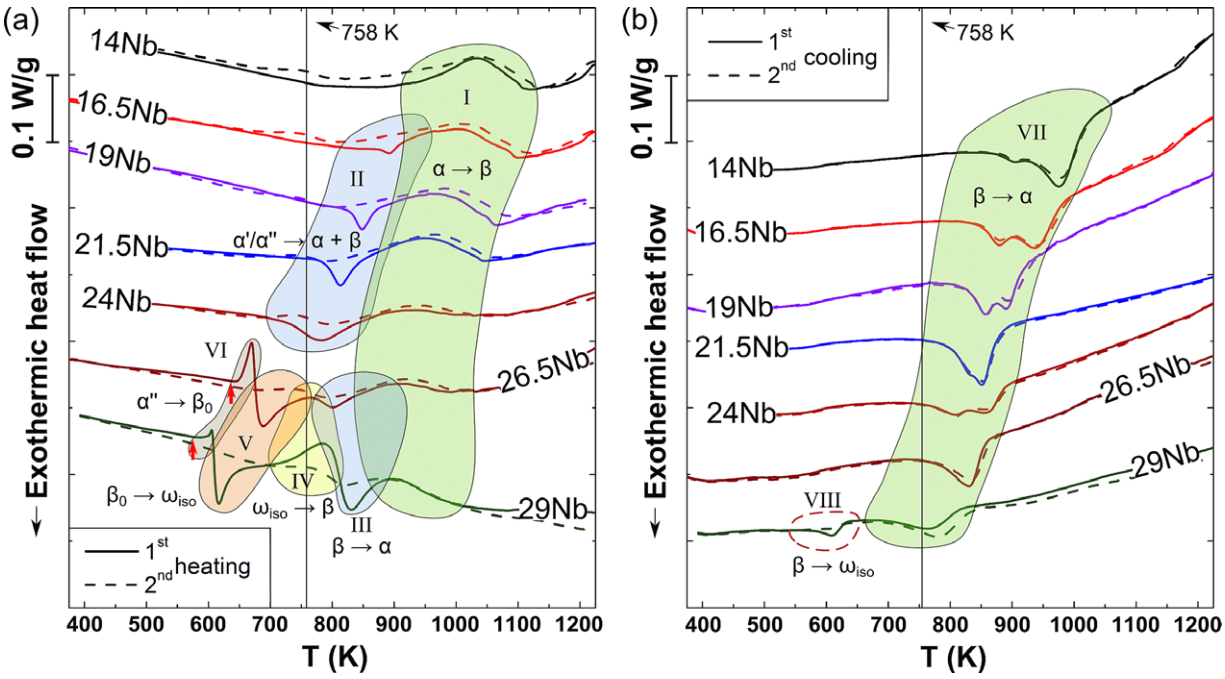

Figure 3. DSC scans of homogenized and water quenched alloys during the first two cycles: (a) first and second heating, (b) first and second cooling.

Table 2. Overview of specimens used for phase analysis after additional heat treatment.

Alloy (wt%)	Specimen	Heat treatment	Resulting phases
Ti–14Nb	P1[a]	↑ 1420 K ↓ RT(10 K min^{-1})	$\alpha+\beta$
Ti–21.5Nb	P2[b]	↑ 813 K + WQ	$\alpha''+\beta+\alpha$
	P3[a]	↑ 1420 K ↓ RT(10 Kmin^{-1})	$\alpha+\beta(+\alpha'')$
Ti–29Nb	P4[b]	↑ 550 K + WQ	α''
	P5[b]	↑ 670 K + WQ	$\beta+\omega_{iso}$
	P6[b]	↑ 818 K + WQ	$\alpha''+\beta+\alpha$
	P7[b]	↑ 1420 K ↓ 670 K + WQ	$\beta+\alpha+\alpha''$
	P8[a]	↑ 1420 K ↓ RT(10 Kmin^{-1})	$\beta+\alpha(+\alpha'')$

[a] Heat treated in the DSC.
[b] Heat treated in the furnace.

presence of non-transformed β proving that α had formed in a diffusional manner during cooling. Still the possibility exists that some β transformed martensitically into α' , which might also explain the low temperature shoulder at 900 K in the DSC signal during cooling. No significant length change was detected by dilatometry for neither $\alpha \rightarrow \beta$ nor the reverse $\beta \rightarrow \alpha$ transformations that might relate to changes of the average atomic volume due to compositional changes. The lattice parameters of α' in the initial state (figure 1) and α after cycling (figure 5(a)) were both $a = 0.2954$ nm and $c = 0.4698$ nm within the limits of experimental error. Brown and Jepson [34] demonstrated in the case of Ti–17.7Nb that cooling rates higher than 6000 K min^{-1} are necessary to determinate the martensitic start temperature M_s. For lower cooling rates the M_s point shifted to higher temperatures suggesting a diffusional component in the transformation. Based on Browns observation and the fact that for Ti–14Nb higher Nb diffusivities at M_s are expected, the reflections in figure 5(a) were indexed with α.

3.3.2. Ti–21.5Nb. The first cycles of DSC- and dilatometry-scans of Ti–21.5Nb together with the Ti-Nb phase diagrams are presented in figure 6. Heating up to the peak temperature of the exotherm at 813 K resulted in a mixture of $\alpha'' + \beta + \alpha$, α'' being the main phase with about 40 vol% (figure 5(b)). Based on this observation the exothermic event at 813 K was assigned to the decomposition α'' into $\alpha + \beta$. It can be ruled out that α' formed upon quenching from 813 K, that had followed heating, because M_s ($\beta \rightarrow \alpha'$), the martensite start temperature for the formation of α' from β, lies around 100 K higher. It is not clear whether the precipitation of α and β from α'' is complete at 813 K, because α'' could have formed from β during quenching that had followed heating to 813 K. The transformation sequence of α'' in Ti–21.5Nb during heating can be summarized as $\alpha'' \rightarrow \alpha + \beta \rightarrow \beta$. The exotherm during cooling, lying above the maximum temperature of stability for ω of 758 K and below the β-transus at 970 K, is caused by the diffusional formation of α from β. The presence of both phases was

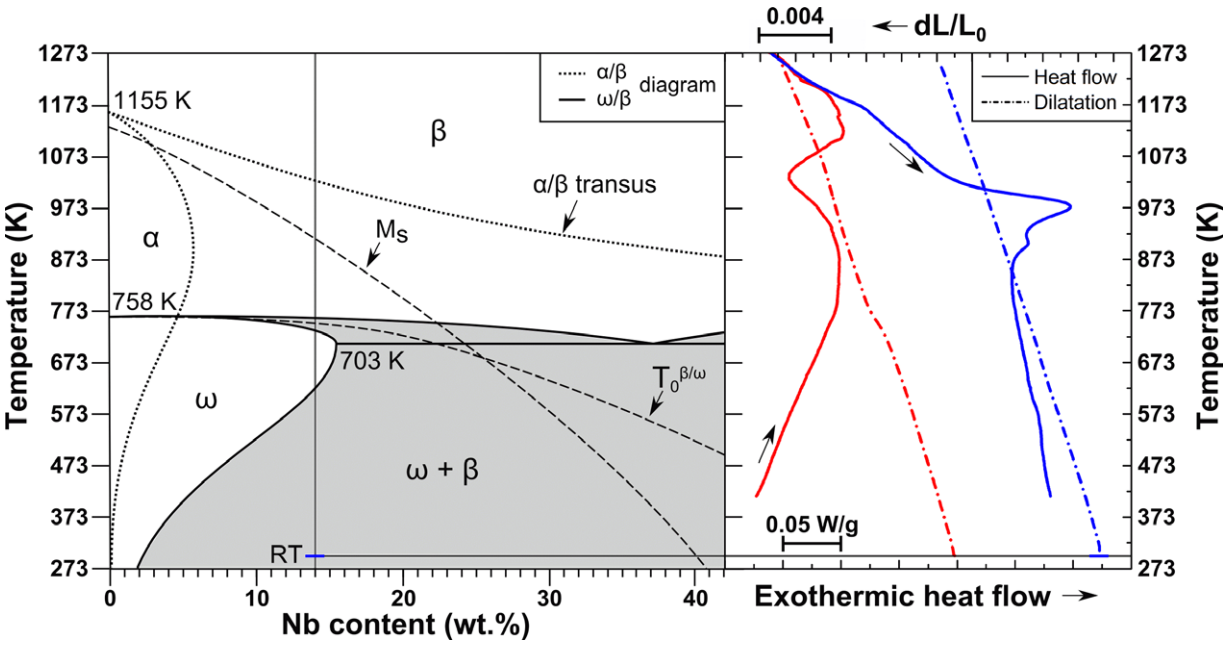

Figure 4. First DSC and dilatometry cycles (right) of Ti–14Nb in relation to the Ti–Nb phase diagrams (left). Dotted lines belong to the equilibrium α/β diagram. Gray areas represent the miscibility gaps in the metastable ω/β phase diagram.

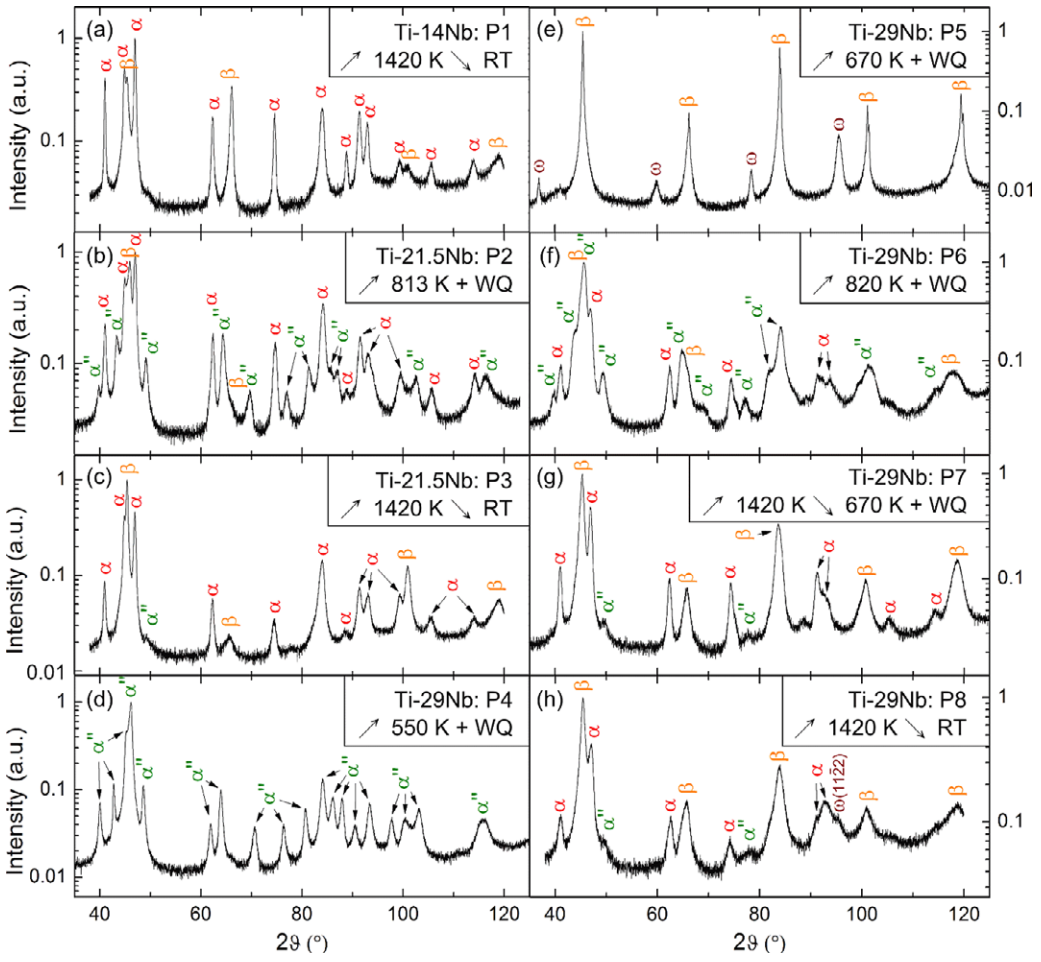

Figure 5. XRD-patterns of heat-treated Ti–Nb alloys. (a) Ti–14Nb, (b)–(c) Ti–21.5Nb and (d)–(h) Ti–29Nb. Intensities are plotted logarithmically for better visibility of low intensity reflections.

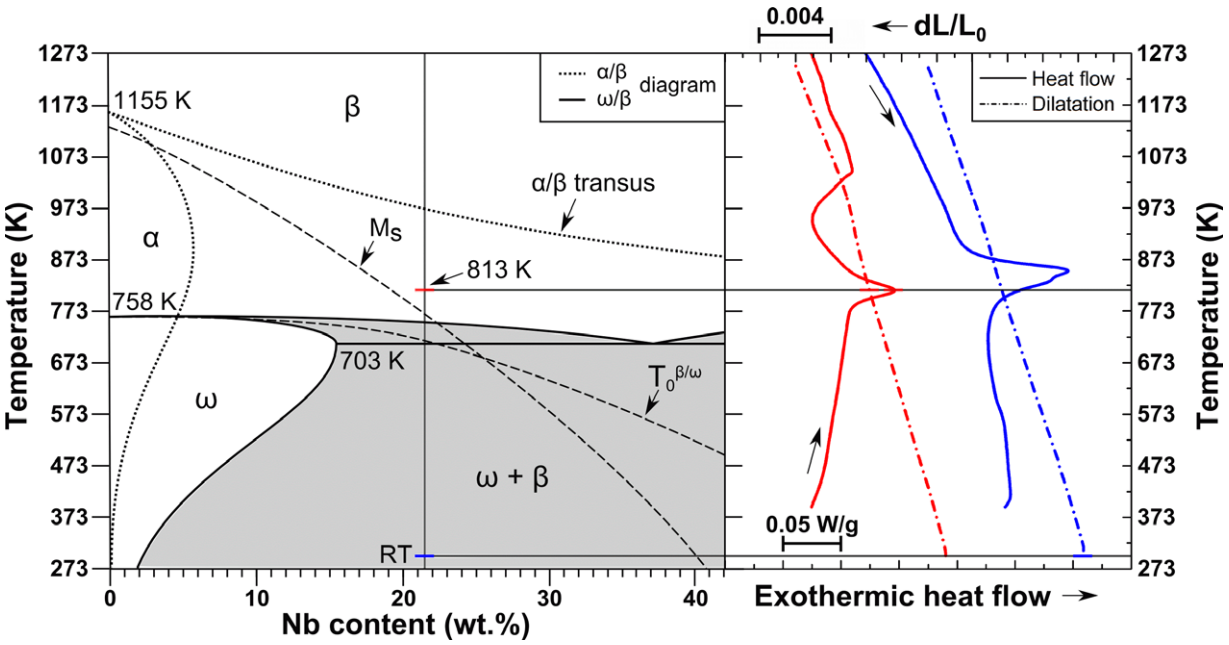

Figure 6. First DSC and dilatometry cycles (right) of Ti–21.5Nb in relation to the Ti–Nb phase diagrams (left). Gray areas represent the miscibility gaps in the metastable ω/β phase diagram.

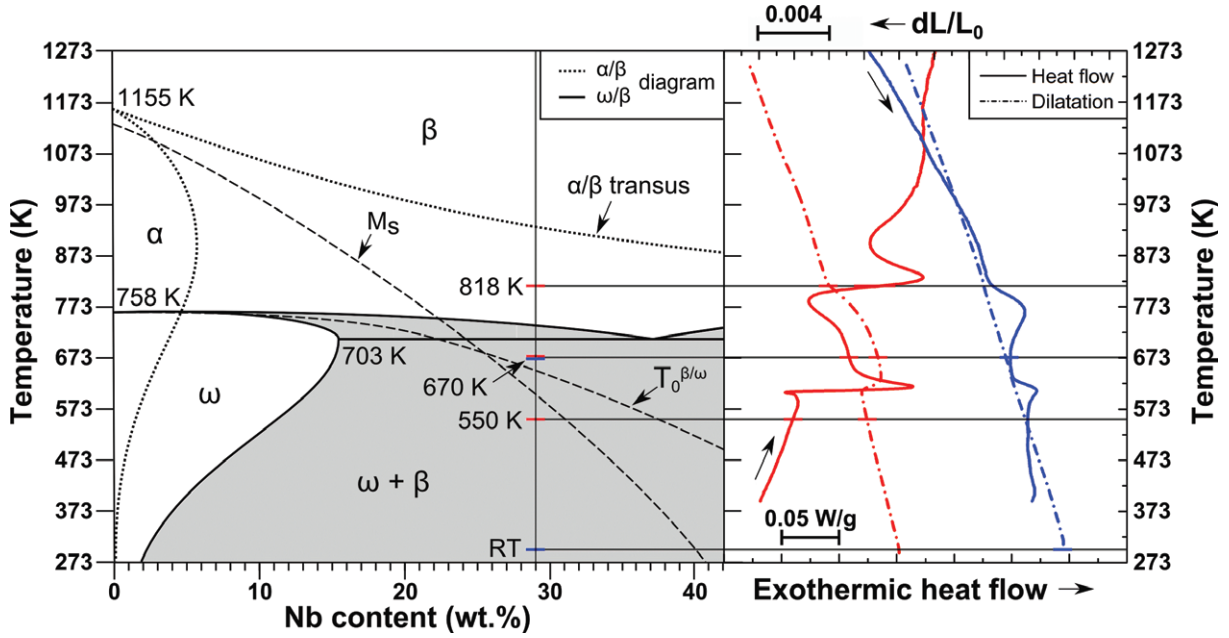

Figure 7. First DSC and dilatometry cycles (right) of Ti–29Nb in relation to the Ti–Nb phase diagrams (left). Gray areas represent the miscibility gaps in the metastable ω/β phase diagram.

confirmed by XRD after one cycle, as can be seen from figure 5(c), and only two small peaks of α'' were detected, the corresponding volume fraction being a few per cent at maximum. Hence lowering of M_s ($\beta \rightarrow \alpha''$) due to enrichment of β with Nb during α precipitation progresses slightly more slowly than specimen cooling on average, so that eventually the specimen temperature fell below M_s ($\beta \rightarrow \alpha''$) and a minor fraction of α'' was formed. Because an $\alpha + \beta$ microstructure was already formed during cooling the exotherm at 813 K did not recur upon second heating (figure 3(a)). Similar to Ti–14Nb, dilatometry-scans did not show significant length changes neither on heating nor cooling.

3.3.3. Ti–29Nb. The first cycle heating and cooling responses detected by DSC and dilatometry of Ti–29Nb together with the Ti–Nb phase diagrams are shown in figure 7. The initial phase constitution of martensitic α'' phase is conserved upon heating to 550 K as can be seen from figure 5(d). Heating above the endotherm–exotherm doublet to 670 K results in a drastic change in phases observed, i.e. a two phase mixture consisting entirely of $\beta + \omega_{iso}$ was

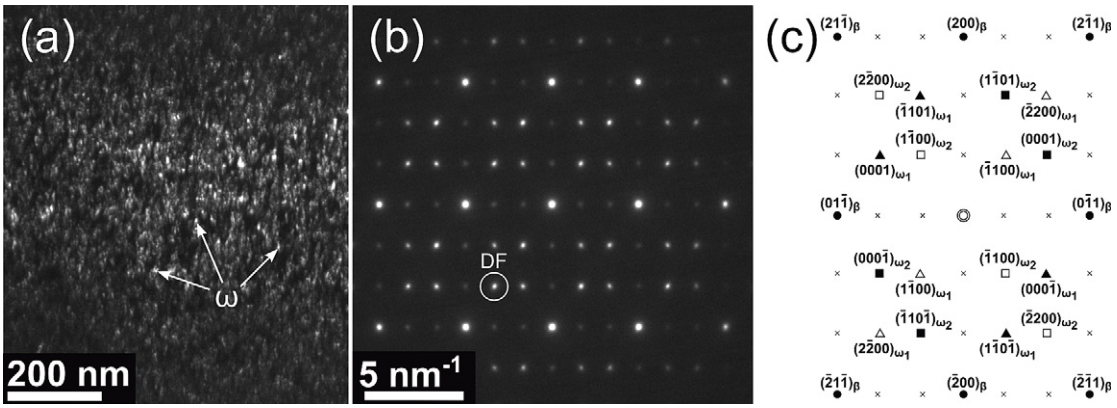

Figure 8. (a) Dark-field (DF) TEM image of ω_{iso} precipitates and (b) the corresponding selected area electron diffraction pattern exhibiting sharp reflections of two ω variants as well as pronounced double diffraction. The beam direction was parallel to [011] of β and [11$\bar{2}$0] of both ω variants. The reflection used for imageing the ω_{iso} precipitates in (a) is marked by a circle. In the key diagram (c) primary reflections are represented by filled symbols, open symbols and crosses represent reflections caused by double diffraction.

found (figure 5(e)). The corresponding lattice parameters were determined as $a_\beta = 0.3277$ nm, $a_\omega = 0.4657$ nm and $c_\omega = 0.2826$ nm. Dark-field TEM imaging shows that the ω_{iso} precipitates form a homogeneous distribution inside the β matrix, as demonstrated in figure 8(a). From these images the diameter of the ω_{iso} particles was estimated to range from a few nm to 30 nm. Selected area electron diffraction (SAED) patterns exhibit sharp ω reflections as shown in figures 8(b) and 8(c), indicating that the collapse of $\{222\}_\beta$ planes which creates the hexagonal ω lattice from β is complete [35, 36]. Since reverse martensitic transformations are endothermic reactions, whereas the formation of ω_{iso} from β is associated with heat release — like any precipitation process based on diffusional demixing of chemical species is — peak VI in figure 3(a) was assigned to the reverse martensitic $\alpha'' \rightarrow \beta_0$ transformation. The reaction being endothermic tells us it proceeds in a chemistry conserving displacive way, thus at least parts of α'' transform back to the parent β phase of the same stoichiometry, designated β_0. A value for the austenite start temperature A_s of 577 ± 3 K was determined from the DSC scan. The reverted β_0 is metastable against chemical demixing leading to precipitation of either ω_{iso} or α. By *in situ* XRD heating experiments of Ti–30Nb Lopes *et al* [37] observed the $\alpha'' \rightarrow \beta_0$ reversion and saw formation of α upon further heating. Figure 3(a) demonstrates that $\alpha'' \rightarrow \beta_0$ reversion in Ti–29Nb is immediately followed by the exothermic formation of ω_{iso} (labeled V). Yet, the question remains open whether all ω_{iso} formed from the freshly created β_0 or parts of α'' decomposed directly into β and ω_{iso}, without the intermediate formation of β_0. Mantani and Tajima [23] observed a similar endotherm–exotherm doublet in Ti–25Nb and recorded a monotonous hardness increase on ageing for 480 s at about 10 K above the exothermic peak. Ageing for longer times resulted in a slight decrease of hardness and the presence of a two phase $\alpha + \beta$ constitution. This suggests that in our case the β/ω_{iso} metastable equilibrium was not reached yet and that $\beta + \omega_{iso}$ would eventually transform into $\beta + \alpha$ on prolonged ageing.

On coming back to figure 7, one can see that heating a specimen (P6) to 818 K caused α reflections to appear as well as α'' reflections to reappear, and conversely β reflections to shrink and ω_{iso} reflections to vanish (figure 5(f)). Two reactions could have possibly caused metastable ω_{iso} to disappear during heating from 670 to 818 K: (i) the gradual endothermic conversion of ω_{iso} into β upon heating through the two-phase ω-β region above 703 K in figure 7 and (ii) the exothermic transformation of ω_{iso} into more stable α. However, the DSC results in figures 3(a) and 7 show a net endothermic heat flow between 670 and 818 K providing evidence for $\omega_{iso} \rightarrow \beta$ being the dominant reaction in this temperature interval. The β thus created is in a metastable state against chemical demixing into equilibrium α and β phases. Accordingly, further heating brings about α to precipitate exothermally as figure 5(f) illustrates. The presence of α'' and concurrent reduction of β reflections can be easily understood by taking the rapid cooling by water quench, succeeding heating to 818 K, into consideration. The dilatometric heating response presented in figure 7 shows a negative length change during ω_{iso} formation, the interval of which corresponds perfectly with the exothermic DSC signal V. This contraction is caused by the progressive reduction of c_ω during approaching the metastable ω_{iso}/β equilibrium [3]. Vice versa the opposite $\omega_{iso} \rightarrow \beta$ transformation is accompanied with dilatation, see figure 7. To sum up, the phase transformation sequence observed in Ti–29Nb during isochronal heating with 10 Kmin^{-1} can be written as $\alpha'' \rightarrow \beta_0 \rightarrow \beta + \omega_{iso} \rightarrow \beta \rightarrow \beta + \alpha \rightarrow \beta$.

On first cooling two exothermic events were detected by DSC. Heating a specimen (P7) to 1420 K and cooling down to 670 K results in a $\beta + \alpha + \alpha''$ phase constitution, as illustrated by figure 5(g). However, as can be seen from figure 5(h) after one full DSC cycle only marginal fractions of α'' are observed, indicating the martensite in specimen P7 formed by water quenching from 670 K. Thus the first exotherm (830 to 670 K) stems from the diffusional $\beta \rightarrow \alpha$ reaction. The fact that only a negligible volume fraction of martensite formed on cooling is confirmed by the second DSC heating scan shown in figure 3(a) which does not exhibit the endothermic $\alpha'' \rightarrow \beta_0$ reversion. Similar observations were made by other authors, who performed second heating runs after cooling

with 10 $Kmin^{-1}$ [37, 38]. The second exotherm (640 to 540 K) in Ti–29Nb during cooling in figure 7 was tentatively ascribed to the formation of ω_{iso} due to a slight intensity increase of the $(11\bar{2}2)_{\omega}$ reflection in the XRD pattern, which is presented in figure 5(h).

4. Conclusions

The thermal stability and transformation behavior of seven binary Ti–Nb alloys with nominal Nb contents ranging from 14 to 29 wt% was studied with DSC, dilatometry, XRD, SEM and TEM. Alloys with 34 wt% Nb or less undergo the same transformation sequences on heating: $\alpha'/\alpha'' \rightarrow \alpha + \beta \rightarrow \beta$. The initial quenched-in martensites decompose into the equilibrium phases α and β, and α progressively transforms into β as the temperature is increased through the α/β miscibility gap. Alloys with Nb contents larger than 24 wt% show considerably different transformation sequences on heating, which can be summed up as $\alpha'' \rightarrow \beta_0 \rightarrow \beta + \omega_{iso} \rightarrow \beta \rightarrow \beta + \alpha \rightarrow \beta$. This is due to the stability of the orthorhombic α'' martensite against decomposition into α and β phases up to the reverse martensitic transformation temperature A_s in these compositions. However the reversion of α'' results in the formation of Nb lean β_0 which is highly unstable against precipitation of ω_{iso}. It is this instability that inhibits the occurrence of a cyclic stable SM effect in alloys of these stoichiometries. At about 758 K the ω_{iso} domains transform into β, which then starts to grow α precipitates on further heating, which in turn revert back to β on approaching the β-transus. On cooling Ti–(14–29)Nb alloys down from the single phase β domain with 10 $Kmin^{-1}$ α precipitates form leading to enrichment of β with Nb and concomitant lowering of M_s resulting in only marginal amounts of α'' martensite to form in alloys containing 21.5 wt% Nb or more. These findings might be used for the development of new heat treatment protocols and establishing reasonable production processes for biomedical Ti–Nb-based devices.

Acknowledgments

The authors thank J van Humbeeck and M Stoica for stimulating and helpful discussions and M Frey, S Donath, V Efimova and A Pöhl for technical support. Funding by the European Commission within the framework of FP7/2007-13 grant agreement no. 264635 (BioTiNet-ITN) and DFG-TR79 is gratefully acknowledged.

References

[1] Lütjering G and Williams J C 2007 *Titanium* 2nd edn (Berlin: Springer)
[2] Leyens C and Peters M (ed) 2003 *Titanium and Titanium Alloys* (Weinheim: Wiley-VCH)
[3] Banerjee S and Mukhopadhyay P 2007 *Phase Transformations — Examples from Titanium and Zirconium Alloys* (Amsterdam: Elsevier)
[4] Niinomi M and Nakai M 2011 *Int. J. Biomater.* **2011** 836587
[5] Geetha M, Singh A K, Asokamani R and Gogia A K 2009 *Prog. Mater. Sci.* **54** 397
[6] Maeshima T and Nishida M 2004 *Mater. Trans.* **45** 1096
[7] Tomio Y, Furuhara T and Maki T 2009 *Mater. Trans.* **50** 2731
[8] Kim H Y, Ikehara Y, Kim J I, Hosoda H and Miyazaki S 2006 *Acta Mater.* **54** 2419
[9] Eisenbarth E, Velten D, Müller M, Thull R and Breme J 2004 *Biomaterials* **25** 5705
[10] Hanada S, Ozaki T, Takahashi E, Watanabe S, Yoshimi K and Abuyima T 2003 *Mater. Sci. Forum* **426–432** 3103
[11] Zhang Y L, Liu H S and Jin Z P 2001 *Calphad* **25** 305
[12] Baker C 1971 *Metal Sci.* **5** 92
[13] Fischer H, Vogel B and Welle A 2004 *Minim. Invasive Ther.* **13** 248
[14] Miyazaki S, Kim H Y and Hosoda H 2006 *Mater. Sci. Eng.* A **438–440** 18
[15] Hao Y L, Li S J, Sun S Y, Zheng C Y and Yang R 2007 *Acta Biomater.* **3** 277
[16] Al Zain Y, Kim H Y, Hosoda H, Nam T H and Miyazaki S 2010 *Acta Mater.* **58** 4212
[17] Al Zain Y, Sato Y, Kim H Y, Hosoda H, Tae Hyun Nam and Miyazaki S 2012 *Acta Mater.* **60** 2437
[18] Kim H, Kim W and Lim S 2006 *Scr. Mater.* **54** 887
[19] Hickmann B S 1969 *J. Mater. Sci.* **4** 554
[20] Sikka S K, Vohra Y K and Chidambaram R 1982 *Prog. Mater. Sci.* **27** 245
[21] Davis R, Flower H M and West D R F 1979 *Acta Metall.* **27** 1041
[22] Moffat D L and Larbalestier D C 1988 *Metall. Trans.* A **19** 1687
[23] Mantani Y and Tajima M 2006 *Mater. Sci. Eng.* A **438–440** 315
[24] Li Q, Niinomi M, Nakai M, Cui Z, Zhu S and Yang X 2011 *Metall. Mater. Trans.* A **42** 2843
[25] Clement N, Lenain A and Jacques P J 2007 *J. Mineral Met. Mater.* **59** 50
[26] Prabha A J, Raju S, Jeyaganesh B, Rai A K, Behera M, Vijayalakshmi M, Paneerselvam G and Johnson I 2011 *Physica* B **406** 4200
[27] Buenconsejo P J S, Kim H Y, Hosoda H and Miyazaki S 2009 *Acta Mater.* **57** 1068
[28] Prima F, Vermaut P, Texier G, Ansel D and Gloriant T 2006 *Scr. Mater.* **54** 645
[29] Moffat D L and Kattner U R 1988 *Metall. Trans.* A **19** 2389
[30] Dobromyslov A V and Elkin V A 2001 *Scr. Mater.* **44** 905
[31] Moffat D L and Larbalestier D C 1988 *Metall. Trans.* A **19** 1677
[32] Brown A R G, Jepson K S, Clark D and Eastabrook J 1964 *Nature* **201** 914
[33] Jepson K S, Brown A R G and Gray J A 1970 *The Science, Technology and Application of Titanium: Proc. First Int. Conf. of Titranium (London)* ed R Jaffee and N Promisel (Oxford: Pergamon) pp 677–90
[34] Brown A R G and Jepson K S 1966 *Mém. Sci. Rev. Métall.* **63** 575
[35] Williams J C, de Fontaine D and Paton N E 1973 *Metall. Trans.* **4** 2701
[36] Nag S *et al* 2011 *Phys. Rev. Lett.* **106** 245701
[37] Lopes E S N, Cremasco A, Afonso C R M and Caram R 2011 *Mater. Charact.* **62** 673
[38] Cremasco A, Andrade P N, Contieri R J, Lopes E S N, Afonso C R M and Caram R 2011 *Mater. Des.* **32** 2387